Electrical and Structural Properties of Oxygen-Precipitation Induced Extended Defects in Silicon

C. Claeys, E. Simoen, J. Vanhellemont

▶ **To cite this version:**

C. Claeys, E. Simoen, J. Vanhellemont. Electrical and Structural Properties of Oxygen-Precipitation Induced Extended Defects in Silicon. Journal de Physique III, 1997, 7 (7), pp.1469-1486. 10.1051/jp3:1997200 . jpa-00249658

HAL Id: jpa-00249658
https://hal.science/jpa-00249658

Submitted on 4 Feb 2008

HAL is a multi-disciplinary open access archive for the deposit and dissemination of scientific research documents, whether they are published or not. The documents may come from teaching and research institutions in France or abroad, or from public or private research centers.

L'archive ouverte pluridisciplinaire **HAL**, est destinée au dépôt et à la diffusion de documents scientifiques de niveau recherche, publiés ou non, émanant des établissements d'enseignement et de recherche français ou étrangers, des laboratoires publics ou privés.

J. Phys. III France 7 (1997) 1469–1486 JULY 1997, PAGE 1469

Electrical and Structural Properties of Oxygen-Precipitation Induced Extended Defects in Silicon

C. Claeys (*), E. Simoen and J. Vanhellemont

IMEC, Kapeldreef 75, 3001 Leuven, Belgium

(Received 3 October 1996, revised 13 December 1996 and 14 March 1997, accepted 2 April 1997)

PACS.61.72.Ff – Direct observation of dislocations and other defects (etch pits, decoration, electron microscopy, X-ray topography, *etc.*)
PACS.72.20.Jv – Charge carriers: generation, recombination, lifetime and trapping
PACS.85.40 Qx – Microcircuit quality, noise, performance and failure analysis

Abstract. — Although the oxygen precipitation process has been extensively studied during the last two decades, there still exists controversy concerning the electrical activity of the precipitates and the associated extended defect complexes. Therefore in the present study a unique combination of complementary characterization techniques is used to gain a better insight into the structural and electrical properties of oxygen-precipitation induced extended defects. TEM and LST are used for the structural analyses, while DLTS, PL, lifetime measurements, EBIC analyses and low frequency noise spectroscopy are used for the electrical characterization. The experimental observations are compared with relevant data available in the literature. Strong evidence is given that in clean processed wafers, the dominant recombination activity is associated with the dislocations, rather than with the precipitates themselves.

1. Introduction

Silicon crystals grown by the Czochralski method typically contain between 5×10^{17} and 10^{18} cm^{-3} dissolved oxygen atoms. In the mid-1950s the interest in oxygen in silicon was mainly triggered by the experimental observation of thermal donor formation [1]. A decade later the subject was abandoned for nearly 20 years in order to gain renewed interest around 1980. Nowadays, there still exists controversy on the thermal donor models (see *e.g.* [2]). The fact that oxygen in silicon became the most extensively studied impurity is caused by the fact that it was observed that the amount of oxygen and its radial and axial distribution have a direct impact on the yield of integrated circuits. At the commonly used processing temperatures, the presence of supersaturated interstitial oxygen leads to the formation of silicon oxide precipitates. The morphology of the oxygen precipitates, *i.e.* platelike, octahedral or spherical, depends on the thermal history of the wafer and the anneal temperature. The precipitation kinetics, *i.e.* nucleation and growth behaviour, has been investigated as function of both the silicon material (crystal growth conditions, oxygen and carbon content, thermal history) and the processing conditions (temperature, time and ambient of thermal treatments). Interactions between oxygen and other crystal defects occur *via* homogeneous and heterogeneous nucleation

(*) Author for correspondence (e-mail: claeys@imec.be)

© Les Éditions de Physique 1997

mechanisms. Nowadays, the behaviour of oxygen in silicon is relatively well understood and semi-quantitative precipitation models have been reported in the literature. A recent review on the topic has been published by Bender and Vanhellemont [3].

It is also well known that oxygen precipitates can have both beneficial and harmful effects on the electrical performance of integrated circuits. The mechanical strength of the material improves by the presence of pinning centres, hampering the movement of dislocations [4]. An important discovery was the observation that oxide precipitate defect complexes can serve as internal getter sites for metallic impurities. Especially if the oxide precipitates are only lying beyond the near surface active device region and deeper into the bulk, a strong improvement of the device yield is found due to the so-called internal gettering effect. Although it was already reported in the early 1960's [5,6], the real interest in and industrial use of internal gettering only took off in the mid 1970's. The basic aspects of internal gettering have recently been reviewed by Ewe *et al.* [7]. Extensive work has also been performed on understanding the mechanism of stacking fault formation during thermal processing [3]. Although a huge amount of qualitative data on stacking faults and oxide precipitates is available in the literature, on some fundamental aspects of the oxygen-precipitation induced extended defects such as *e.g.* the origin of their electrical activity (*i.e.* the precipitates themselves, the associated dislocations, or the presence of metallic decoration) controversial models are reported. Therefore the present paper aims at shining new light on the electrical and structural properties of oxygen-precipitation related extended defects by using a variety of complementary analytical tools.

2. Experimental Procedures

2.1. PROCESSING ASPECTS. — Different 125 mm diameter silicon substrates have been used for the present study, *i.e.* Float Zone (FZ), epitaxial and Czochralski (Cz) Si wafers with an interstitial oxygen concentration ranging between 7×10^{17} cm^{-3} and 11×10^{17} cm^{-3}. Details on the wafer type, the doping range and the interstitial oxygen content are given in Table I. These dedicated and well characterized wafers have been divided over different batches which first received a thermal pre-treatment according to one of the three following sequences: i) no thermal treatment (no), ii) an oxygen precipitation nucleation step at 750 °C for 8 h in nitrogen (nucl), and iii) an internal gettering cycle consisting of an oxygen out diffusion step at 1100 °C in 5% O_2 for 6 h followed by the nucleation treatment (IG). Some of the wafers then received a VLSI compatible diode processing, *i.e.* a LOCOS isolation scheme, a field oxidation of 10 h in oxygen at 975 °C during which the already present oxide precipitates further grow, a 80 keV As and 130 keV P ion implantation for forming the n^+p junctions, and standard Al metallisation. Both perimeter diodes with a meander of 10 times 900 μm $\times$ 30 μm and square area diodes of 900 μm $\times$ 900 μm were fabricated. Using total reflection X-ray fluorescence (TXRF) and DLTS, no metallic contamination could be detected neither before nor after processing, indicating that the concentration should be below the detection limit of 10^{10} atoms cm^{-2}. The low metallic content after processing is also in agreement with the low leakage current levels and with the experimental data which are reported in the following sections.

2.2. STRUCTURAL CHARACTERIZATION. — Before and after the diode processing, the interstitial oxygen content was measured with Fourier Transform Infrared (FTIR) spectroscopy. The measurements were done with a Bruker IFS 66v instrument, at the University of Gent, equipped with a cooled MCT detector, by using the IOC-88 calibration factor of 3.14×10^{17} cm^{-3}/cm^{-1} [8]. FTIR measurements at deep cryogenic temperatures (typically at 15 K) also allow to separate the absorption peaks associated with interstitial oxygen from the absorption bands corresponding with different silicon oxide phases.

Table I. — *Parameters of the wafers used in the experimental matrix. For each sample the code, the type and the pre-treatments are indicated in the first 3 columns. The interstitial oxygen content, before and after the full diodes processing respectively, is given in the next two columns. Columns 6, 7 and 8 give the defect density determined by TEM, LST and EBIC respectively. Column 9 indicates the width of the DLZ, estimated from TEM measurements. The effective carrier lifetime at T = 300 K, determined with LIA and MWA, calculated from I-V analyses and by EBIC measurements are given in columns 10 to 13. For the latter case, minority carrier diffusivities of $D_n = 35\ cm^2\ s^{-1}$ and $D_p = 12\ cm^2\ s^{-1}$ were used for the p- and n-type samples, to calculate the lifetime from the diffusion length. The last column gives the current noise spectral density, measured at 1 μA and averaged over different samples on the same wafer.*

sample	type	Anneal	O_i (init) 10^{17} cm^{-3}	O_i (after) 10^{17} cm^{-3}	N_{TEM} 10^9 cm^{-3}	N_{LST} 10^9 cm^{-3}	N_{EBIC} 10^9 cm^{-3}	DLZ μm	LIA μs	MWA μs	$I-V$ μs	EBIC μs	S_{II} 10^{-24} A^2/Hz
T1	p	no	9.3	9 04	1-2	1	0 5	-	8.3	4.2	1.6	0 7 - 1.8	1 9
T2	p	nucl	9.2	-	1-2	1 3	0.4	-	3 8	1 6	0.66	0.4 - 0.7	1 8
T3	p	IG	9.2	8 65	1	0.76	0.1	-	7 4	3.2	7.2	> 3*	-
T26	p	no	11 1	3.0	50	13	6	3	0 46	0 62	0.062	0 2	4 1
T28	p	IG	10.8	3 13	10	7.4	0.8	30	0 68	0 75	0 75	0.7	2 6
T21	n	no	7 3	7 3	< 1	0.011	-	-	15	17	-	-	-
T22	n	nucl	7.3	-	< 1	0 022	-	-	15	24	-	-	-
T23	n	IG	7 2	7 2	< 1	0 022	-	-	17	20	-	-	-
T11	n	no	10 2	6 7	10	7 1	2 5	6	0 72	1.0	-	> 5*	-
T12	n	nucl	10	6 8	10	5 5	1 7	2	0 92	1.2	-	> 8*	-
T13	n	IG	9 9	5 84	3	4 3	0 5	30	1 1	1.1	-	> 8*	-

(-) value not determined,
(*) diffusion length at the limit of EBIC technique

The structural defect characterization is done by Transmission Electron Microscopy (TEM), on cross-sectional samples prepared in the conventional way by grinding, polishing, dimpling and Ar-ion milling. High voltage TEM analyses, performed on the Jeol 1250 microscope of the University of Antwerp (RUCA) with an acceleration voltage of 1000 kV, are used to characterize the bulk defects and to determine the defect density and distribution.

Infrared Light Scattering Tomography (LST) is used as a complementary non destructive tool to determine the density and distribution of bulk defects, and is especially useful for samples with defect densities below 10^{10} cm^{-3} which are difficult to detect with TEM. The main advantage of LST is the wide range of defect densities that can be observed ranging from 10^4 to about 10^{10} cm^{-3} and the fact that one can differentiate between different types of defects such as grown-in defects, oxygen precipitates, prismatic punching systems and stacking faults [9]. For the LST studies, use was made of the facilities at the ISP in Frankfurt/Oder. The MILSA IRHQ-2 instrument from RATOC is equipped with a pulsed YAG-laser of 1060 nm wavelength for the 90° scattering mode and a laser diode of 870 nm wavelength for the Brewster angle illumination mode.

2.3. Electrical Characterization. — Deep-Level Transient Spectroscopy (DLTS) is applied to determine the location in the bandgap and the density and depth profiles of deep levels present within the depletion layer of the devices. In order to characterize the traps in detail, measurements are done over a wide temperature range from 77 to 450 K. DLTS measurements do not allow to detect defect densities lower than 10^{-4} times the doping concentration and can only be performed on samples with either a Schottky or a p-n junction. In the latter case, however, also minority traps are accessible for observation.

Another very sensitive method to study carrier recombination properties of defects is low temperature photoluminescence (PL) [10]. The main advantage of PL is that it does not require any sample preparation which might influence the defect properties. The PL measurements are performed with a modified BIORAD set-up at the Technical University of Delft, based on a Fourier spectrometer and a Ge liquid N_2-cooled detector. An Ar^+ ion laser was used as an excitation source.

The lifetime measurements are done by either the Light induced Infrared Absorption (LIA) technique, Microwave Absorption Measurements (MWA), both at the University of Vilnius, or by evaluating the current-voltage (I–V) characteristics of the diodes. The LIA technique, requiring the removal of the diode structures by etching and mechanical polishing, determines the lifetime of the minority carriers under high carrier injection conditions (about 5×10^{17} carriers cm^{-3}) [11]. The MWA measurements are done at 10 GHz and under moderate injection (about 5×10^{15} carriers cm^{-3}). The excess carriers are generated by a pulsed Nd:YAG laser with a beam of 1.06 μm wavelength. In both cases about 50 μm of silicon is polished away on both sides of the wafer so that information is obtained on only the bulk recombination properties.

An analysis of the forward diode current I_F allows to calculate the recombination lifetime, while the reverse diode current I_R yields the generation lifetime [12]. By analysing diodes with large and small areas and large and small perimeters, one can further differentiate between bulk and surface leakage current components. It has recently been demonstrated that by making the proper corrections for perimeter and diode ideality effects, a good agreement is obtained between the recombination lifetime calculated from the forward I–V characteristics and the one obtained with MWA measurements [13].

The EBIC measurements were performed at ISP, Frankfurt/Oder, by using a Cambridge 360 SEM equipped with an Oxford cold stage and a Matelect Induced Signal Monitor to visualize recombination active defects and to measure the recombination activity between

80 and 300 K. The beam energy was varied between 15 and 40 keV, while the beam current was kept below 50 pA. The minority carrier diffusion length is determined from the decay of the charge collection efficiency between 30 and 40 keV averaging over an area of typical 0.1 ... 0.2 mm^2 [14].

The low frequency noise measurements are done on diodes in forward operation, by using a dedicated home-built system consisting of a low noise pre- amplifier circuit which is powered by a car battery [15]. The system also enables to measure the dynamic resistance of the diode. The LF noise spectrum is measured at room temperature in the range between 1 Hz and 10 kHz by an HP3265 Dynamic Signal Analyser.

3. Experimental Results and Discussion

This section reports on the experimental observations obtained by using the above mentioned structural and electrical characterization techniques. A summary of some typical data that have been obtained is given in Table I. Comments on the different values will be given in the paragraph dealing with that particular technique. Each paragraph first outlines typical results coming out of this work, before wherever relevant making a possible comparison with data published in the literature. A more general discussion of the conclusions obtained by combining the different experiments is given in paragraph 3.3.

3.1. Structural Defect Analysis

3.1.1. FTIR Analyses. — FTIR is used to measure the interstitial oxygen concentration before and after the diode processing. It can be noticed in Table I that the amount of precipitated oxygen depends on both the initial oxygen concentration and the thermal pre-treatment. As mentioned before, FTIR at lower temperatures (*e.g.* at 15 K) allows to differentiate between the absorption bands associated with interstitial oxygen, *i.e.* peaks at 1128, 1138 and 1206 cm^{-1}, and those related to different silicon oxide phases, *i.e.* near 1100 and/or at 1220 cm^{-1}. The first peaks are strongly temperature dependent, while the position and the shape of the latter bands are temperature independent [16]. Typical FTIR spectra for different samples are shown in Figure 1, clearly revealing the precipitated SiO_x phase [17]. Two silicon oxide related precipitate bands are observed, in agreement with the TEM observation of platelike precipitates. The weak peaks in the spectrum of sample T1 may be associated with the single ionised oxygen thermal donor series $TD1^+$, $TD2^+$ and a trace of $TD3^+$ [18]. The TD density is estimated to be of the order of a few times 10^{13} cm^{-3}, which is far below the doping concentration of the samples.

3.1.2. TEM Analysis. — TEM analysis reveals that for wafers with a high initial oxygen content, a Defect Lean Zone (DLZ) is present after the diode processing [19]. The IG sequence results in a DLZ of about 10 μm, while in wafers with no pre-treatment the DLZ is only 3 μm. This is illustrated in the HVEM micrograph shown in Figures 2a and 2b. Deeper in the bulk of the material, as can be clearly seen in the higher magnification image shown in Figure 2c, typical defects such as Precipitate/Dislocation complexes (PD) and isolated Platelike SiO_x precipitates (P) are observed. The PD density is always one order of magnitude higher than the precipitate density. As can be noticed in Table I, the bulk precipitate density N_{TEM} increases for increasing oxygen content of the starting material and for a high oxygen material is always smaller for IG wafers than for wafers without a pre-treatment. The average PD and precipitate size is larger in IG wafers compared to wafers without a pre-treatment, due to the much larger critical precipitate radius in case that a high temperature out-diffusion step is implemented [19]. At high temperatures, only the largest precipitates will continue to grow,

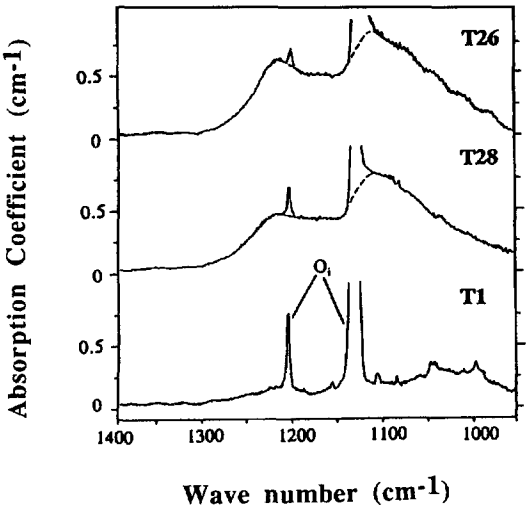

Fig. 1. — FTIR spectra recorded at 15 K of p-type wafers T1 (medium oxygen, no thermal pre-treatment), T28 (high oxygen, IG step) and T26 (high oxygen, no thermal pre-treatment). The 1110 cm^{-1} and 1220 cm^{-1} bands are associated with platelike SiO_x precipitates. The weak structure in the T1-spectrum is due to thermal donors ($TD1^+$ and $TD2^+$).

while the smaller ones are dissolved. The precipitate density shows the inverse trend of that of the radius and is higher in p-type than in n-type substrates.

3.1.3. LST Characterization. — Infrared light scattering tomography is a more suitable technique than TEM to determine the defect density as it is non-destructive, faster and applicable to a wide range of defect densities. Typical illustrations of LST images are shown in Figure 3 for diodes processed on high oxygen n-type material. The higher magnification image illustrates that also stacking faults and prismatic punching systems can be observed and identified [9]. For different oxygen concentrations, the LST densities are in close agreement with those determined by using a preferential defect etch [20]. As can be seen in Table I, there is a good agreement between the N_{TEM} and N_{LST} defect densities. For too large defect densities ($> 10^{10}$ cm^{-3}) LST analysis becomes to difficult due to the overlap of the defects in the image. There is also a strong correlation between the LST density and some electrical parameters such as *e.g.* recombination and generation lifetime, and PL amplitude [21]. This will be illustrated and discussed in the following sections.

3.2. Electrical Defect Characterization

3.2.1. DLTS Analysis. — DLTS is giving information on the signature (bandgap position and capture cross section) of the deep levels present in the depletion layer of the devices. Applying this technique to wafer T26, a high oxygen content p-type wafer without a pre-treatment, two minority traps have been detected, *i.e.* with reference to the conduction band E_c, ET1 at $E_c - 0.23$ eV and ET2 at $E_c - 0.43$ eV [19]. These traps are only observed for a sufficiently large depletion width, much larger than the DLZ width (= 3 μm) observed by TEM. The depth profile of the ET2 density and of the derivative of the leakage current with respect to the depletion depth (dI_R/dW), or in other words the generation centre profile, are as illustrated in Figure 4 falling together. This suggests that most likely the leakage current is dominated by the deep centres associated with ET2.

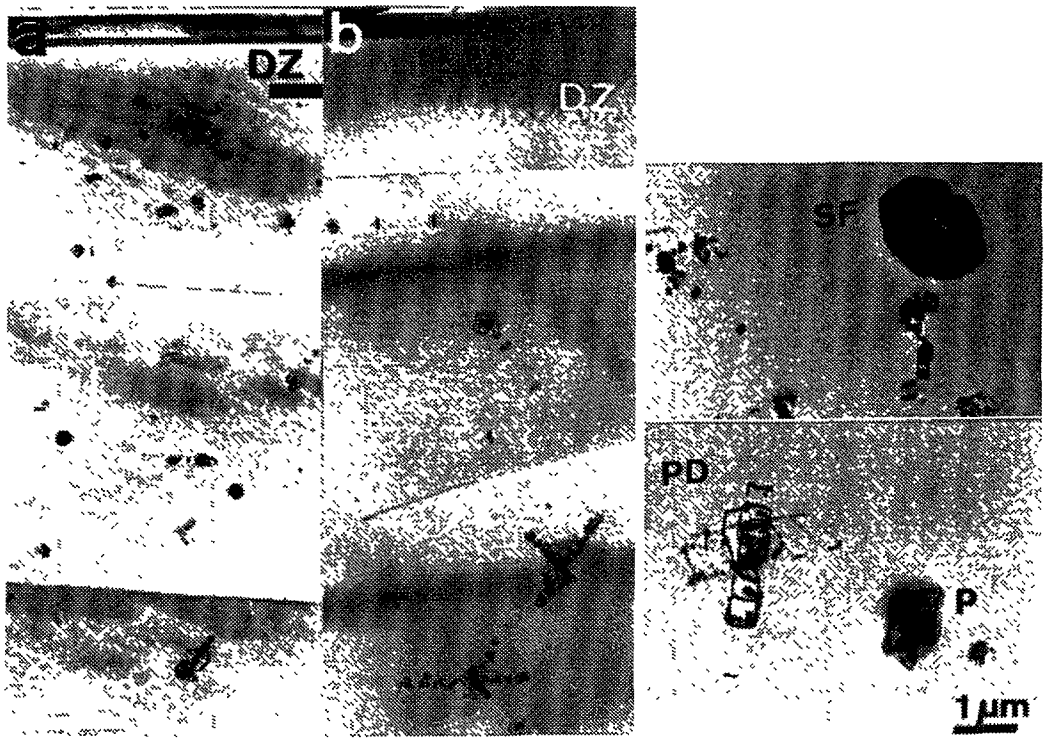

Fig 2. — a), b) HVEM image illustrating the bulk defect distribution in T26 (left, 3 μm DLZ) and T28 (right, 10 μm DLZ). c) Higher magnification TEM micrographs of typical extended defects related with oxygen precipitation: Stacking Fault (SF), oxide Precipitate (P) and Precipitate/Dislocation complex (PD).

In the literature, also Chan *et al.* [22] have reported the observation of a minority carrier trap located at $E_c - 0.43$ eV in their high oxygen p-type substrates after a low/high temperature treatment. Although care has to be taken to compare results obtained on different material and after a different processing cycle, also in his case oxygen-precipitation related extended defects are involved. In our samples, deep levels could only be observed in T26, as in the other samples either the defect density was too low, or the defects were outside the probed area.

3.2 2. Photoluminescence Studies. — Some typical PL spectra for p and n-type wafers with different oxygen concentrations are shown in Figure 5. Beside the TO-phonon replica of the boron- or phosphorous-bound exciton peak, the main features in the spectra are the D1 and D2 lines at 807 and 874 meV, respectively [23]. These D-bands, of which the intensity depends on the initial oxygen content of the material, have been reported in the literature and may be related to either impurity related optical transitions in the vicinity of the dislocation core or to intrinsic properties of the dislocation itself [24]. Although Lelikov *et al.* [25] have suggested that the position of the PL lines are associated with the edge component of the Burgers vector of the dislocation, no evidence of this is obtained in the present work.

A detailed study of the use of PL for the determination of the dislocation structure is out of the scope of the present paper. For the sake of completeness it can be mentioned that

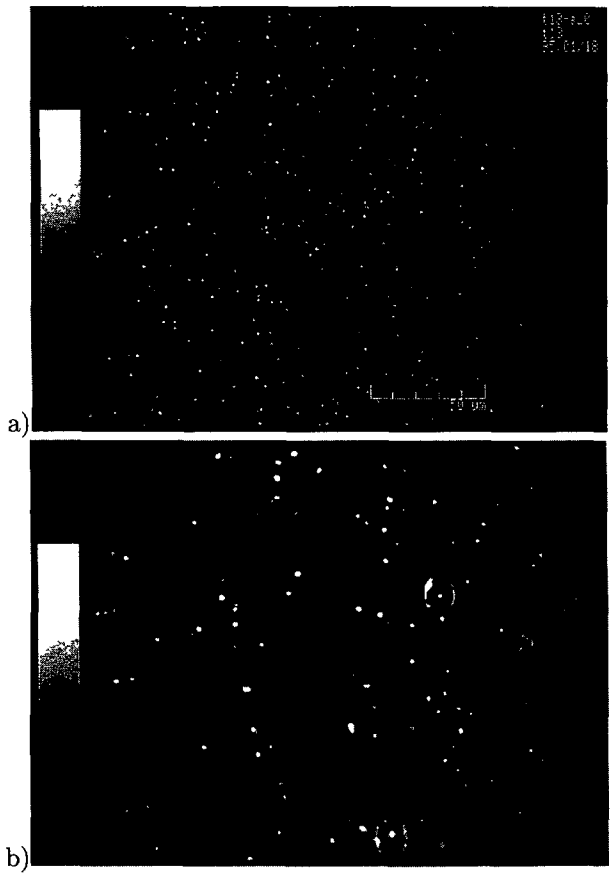

Fig. 3. — LST images of a high oxygen n-type sample (T13). The higher magnification (b) illustrates the presence of stacking faults and prismatic punching systems.

Wijaranakula [26] postulated a model whereby the D1 and D2 lines are associated with the edge and screw components of the oxygen-related extended dislocation loops, respectively. In that model, however, an interaction between the dislocation segments and impurities is required, so that in low oxygen material without contamination (*e.g.* Cu or Zn) no D-bands are observed. This is not in contradiction with the observations of the present study. It is believed that the position of the D-lines is determined by the dislocations, while the intensity of the lines is triggered by the contamination level.

3.2.3. Lifetime Measurements. — In the frame of the present study, measurements of the carrier lifetime have been done at moderate and high excitation levels by using the microwave and infrared absorption technique, respectively. In addition, analysis of both forward and reverse current-voltage ($I-V$) has been used to determine the recombination and generation lifetime. The effective recombination lifetime is influenced by both surface recombination effects and bulk recombination, and only in the case where the surface recombination can be neglected, the effective lifetime can be assumed to be equal to the bulk lifetime. Surface passivation techniques are often used to suppress the surface recombination. The bulk recombination

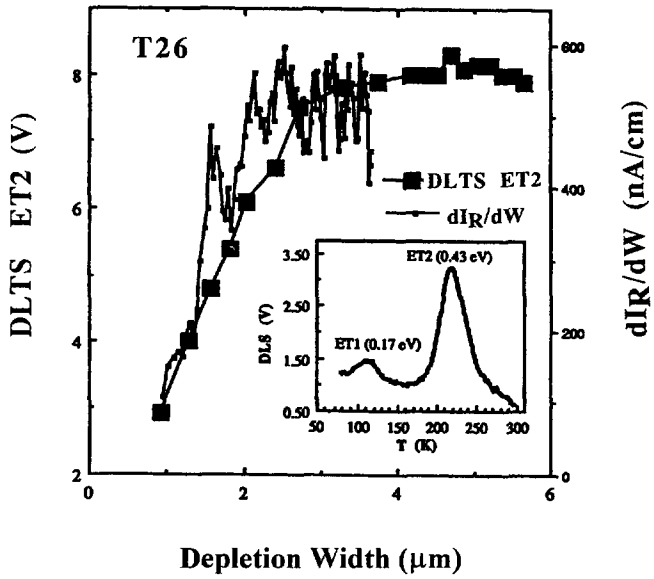

Fig 4. — Depth profile of the density of the minority ET2 trap and of the derivative of the leakage current (dI_R/dW) with respect to the depletion width for a high oxygen content wafer with 5×10^{10} cm^{-3} oxygen-related precipitate/dislocation complexes (PDs). The Defect Lean Zone is about 3 μm near the wafer surface. The insert gives the DLTS spectrum with the ET1 and ET2 minority traps.

lifetime τ_b depends on the carrier injection level and can in general be expressed as [27]

$$\frac{1}{\tau_b} = \frac{1}{\tau_{SRH}} + \frac{1}{\tau_{rad}} + \frac{1}{\tau_{Auger}} \tag{1}$$

with τ_{SRH}, τ_{rad} and τ_{Auger} the Shockley-Read-Hall (SRH), the radiative and the Auger lifetime component respectively. For not too high injection levels, as used in MWA, the radiative and Auger components may be neglected, so that the bulk lifetime is mainly determined by the SRH component. In the low injection limit, the SRH lifetime is inversely proportional to the concentration of recombination centres N_T and their capture cross section σ_n and is given by [27]

$$\tau_{SRH} = \frac{1}{\sigma_n v_{th} N_T} \tag{2}$$

with v_{th} the thermal velocity of the carriers. It has to be remarked that both MWA and LIA are giving a bulk lifetime averaged over the wafer thickness. This is not the case for the lifetime determined from diode characteristics, where the lifetime is corresponding to the value in the near surface active device region.

Table I shows that from the MWA and LIA measurements follows that the carrier lifetime decreases for increasing oxygen content of the starting material. This is also illustrated in Figure 6, giving for both n- and p-type wafers the bulk lifetime (determined by three different techniques) as a function of the initial oxygen content. In first approximation, there is an exponential dependence of the carrier lifetime on the oxygen concentration. There is also a rather good agreement between the lifetime values obtained by the different techniques.

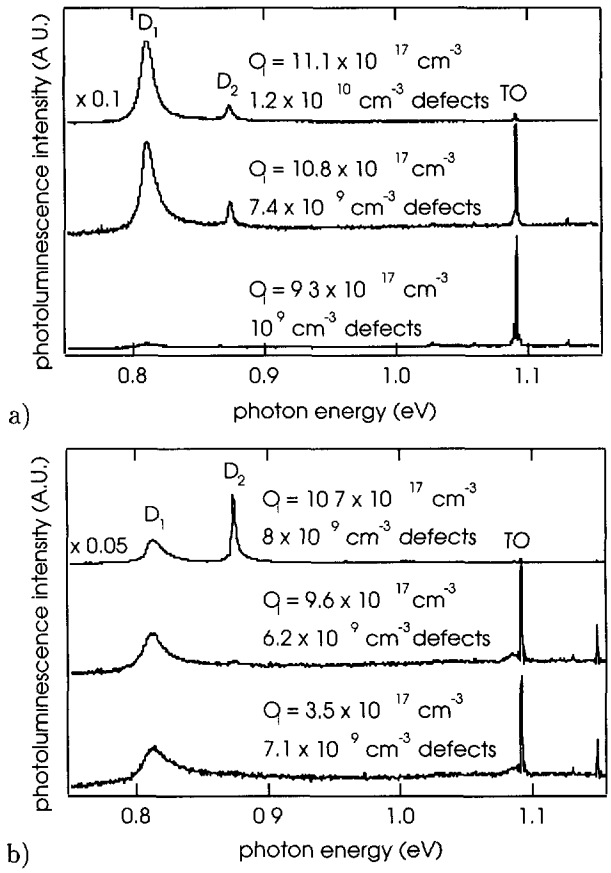

Fig 5 — PL spectra measured at 4.2 K of p-type (a) and n-type (b) samples with different interstitial oxygen concentrations O_i and LST defect densities. TO is the TO-phonon replica of boron- or phosphorous bound exciton PL. D1 and D2 are PL lines related to the oxygen-precipitation induced extended defects.

For high oxygen material, the IG sequence increases the carrier lifetime. The effect is not pronounced in the MWA and LIA data as these techniques are measuring average bulk lifetimes over the whole wafer thickness

A quite interesting observation is the correlation between the inverse carrier lifetime and the LST defect density as illustrated in Figure 7a for the MWA lifetime and in Figure 7b for the generation and recombination lifetime obtained from diode measurements [21]. Figure 7a clearly shows that there is a correlation between the lifetime and the defect density for wafers which received the same thermal processing. There can, however, be a large difference in lifetime for wafers with the same defect density observed by LST but a different thermal history, as pointed out by the circle in Figure 7a. This point has been obtained by investigating wafers which received a special two-step anneal treatment in order to reduce the size of the precipitates and therefore to suppress the associated generation of extended defects. This indicates that not the precipitate concentration itself (LST is mainly measuring SiO_x precipitates) is dominant for the lifetime, but rather the density, the type and state (*i.e.* core structure and possible decoration with impurities) of the dislocations. By controlling the extended defect density, the lifetime can thus be optimised. Figure 7b allows to estimate the bandgap position (E_T)

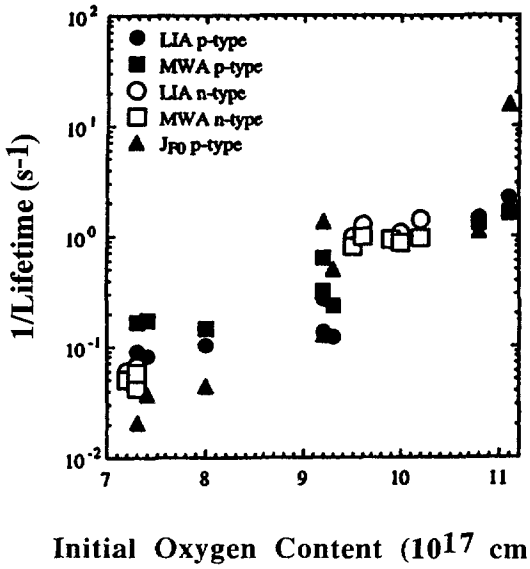

Fig. 6. — Inverse of the recombination carrier lifetime measured by electrical and optical/microwave measurements as a function of the initial oxygen content. An exponential relation between both parameters is observed.

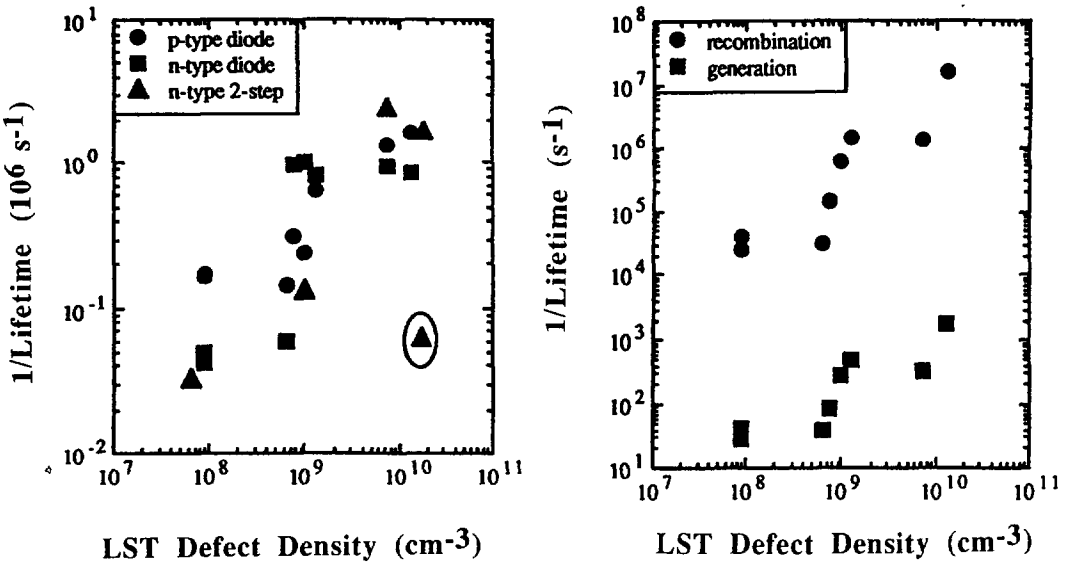

Fig. 7. — a) Inverse carrier lifetime determined with MWA as a function of N_{LST}. For samples with similar extended defects, a linear correlation is obtained. The sample with much less dislocations per precipitate (encircled triangle) jumps out. b) Inverse τ_g and τ_r determined from $I-V$ characteristics on p-type substrates as a function of N_{LST}.

of the dominant trapping centre. In case that there is one dominant trapping centre active, the relation between the recombination (τ_r) and the generation lifetime (τ_g) in first order approximation is given by [28]

$$kT \ln\left(\frac{\tau_g}{\tau_r}\right) = |E_T - E_i| \tag{3}$$

with E_i the intrinsic level. Straightforward calculation based on the ratio of the two lifetimes leads to a trapping centre at either $E_v + 0.4$ eV or $E_c - 0.4$ eV.

3.2.4. EBIC Measurements. — EBIC is a complementary technique to determine the electrical activity of the defects. The recombination activity of the defects will locally reduce the number of e-beam induced carriers. By measuring the diffusion length, one can also determine the minority carrier lifetime. The diffusion length of the material L has two components, *i.e.* a component related to extended defects L_{def} and a background component L_b, so that the general expression for the diffusion length becomes [29]

$$L^{-2} = L_{def}^{-2} + L_b^{-2} \tag{4a}$$

with L_{def} determined by the minority carrier diffusivity D and the bulk lifetime τ_b

$$L_{def} = \sqrt{D\ \tau_b}. \tag{4b}$$

For the first order calculations a minority carrier diffusivity of $D_n = 35$ cm^2 s^{-1} and $D_p = 12$ cm^2 s^{-1} for the p- an n-type samples, respectively, has been assumed. In general there is a good agreement between the lifetime determined by EBIC and those obtained by other techniques. Only for high diffusion lengths, the EBIC measurements are becoming unreliable. Similar to other analytical techniques, the electrical activity of the defects can be influenced by cooling the samples. However, the observation that by cooling from 300 to 80 K the image contrast enhances seems to indicate that the recombination contrast of the oxygen precipitation induced extended defects is controlled by shallow levels, rather than by deep levels [29]. This observation is only seen for "clean" wafers. In case that the wafers are intentionally contaminated with Fe, deep level traps are observed, characterized by a low diffusion length and a marked electrical activity at room temperature. Recently, other evidence has been reported in the literature that clean dislocations are electrically inactive at room temperature and show a strong electrical activity at 80 K, while for contaminated dislocations the electrical activity decreases upon cooling [30].

EBIC not only gives information on the electrical activity of the defects, but can also be used to estimate the defect density. As shown in Table I, the N_{EBIC} density is always lower than the N_{TEM} and N_{LST} values. The reason for this is not clear, but may be related to: i) an inhomogeneous defect distribution over the whole wafer thickness, ii) the fact that for the different techniques the probing depth is quite different, iii) differences in carrier concentrations, or iv) a lower electrical active defect density compared to the total defect concentration in the material.

3.2.5. Low Frequency Noise Evaluations. — The LF noise characteristics of devices are much more sensitive than many other electrical parameters, so that noise diagnostics is more and more used for yield assessment and quality and reliability predictions. Noise spectroscopy is also able to determine the signature of trapping centres. Therefore the authors have recently reported on LF noise studies of the generation-recombination activity of extended defects [31]. The LF excess noise of state of the art n^+p junction diodes can empirically be modelled as [31]

$$S_I = C\frac{I_F^\beta}{f^\gamma} \tag{5}$$

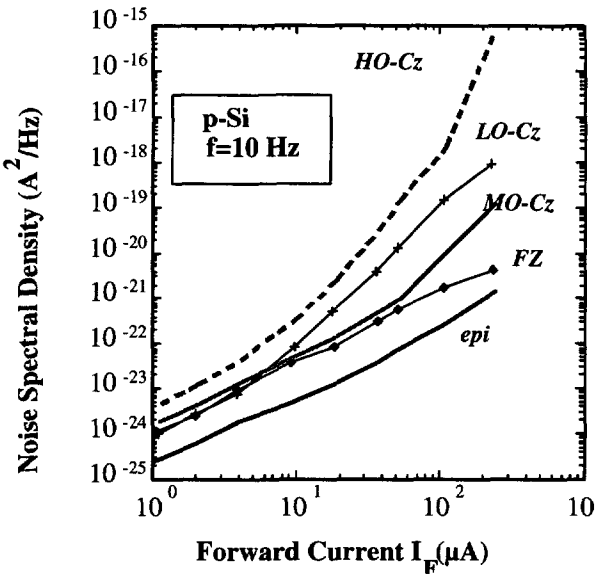

Fig. 8. — Current noise spectral density at $f = 10$ Hz as a function of the forward diode current I_F, for n^+p diodes fabricated on different substrates. The Cz substrates received no pre-treatment.

with S_I the current noise spectral density, I_F the forward diode current, f the frequency, and C an empirical coefficient. The frequency exponent is in the range $0.6 < \gamma < 1.2$, while for the current exponent the $1.5 < \beta < 2$ range is found. This current dependence of the noise spectral density is typically observed for trap-assisted generation-recombination centres. The impact of the substrate quality on the noise spectral density is illustrated in Figure 8. The lowest noise figures are obtained for epitaxial and FZ wafers, while an increased noise level is observed for Cz wafers. The impact of the substrate quality becomes more pronounced at higher current levels. Figure 9 gives for two different current levels, the noise spectral density as a function of the initial oxygen concentration. The noise level increases for increasing current levels, as indicated by equation (5) and for higher initial oxygen concentrations. However, it has to be remarked that an IG pre-treatment reduces the noise compared to wafers with a similar oxygen content but without a pre-treatment. As in general, both perimeter and bulk effects have to be taken into account, (111) oriented wafers are more noisy than (100) substrates [32]. The latter have less interface traps along the edges of the isolation region.

In order to get a better insight into the impact of the substrate quality on the LF noise behaviour, experimental data obtained by the different analytical techniques mentioned above have been put together. First of all, a clear correlation is found between the noise spectral density and the defect density determined by LST, as shown in Figure 10a [33]. For low bulk defect densities, the noise is nearly independent of the defect concentration, indicating a "surface recombination" origin. However, for higher defect levels the noise increases with increasing bulk defect density. This clearly points towards the recombination activity of the oxygen precipitation induced extended defects, resulting in a GR based $1/f$ noise origin. There also exists a correlation between the noise spectral density and the inverse recombination lifetime, as can be seen in Figure 10b. For high lifetime values the noise is not correlated, but there is a clear trend for low lifetime material, *i.e.* material with a higher defect density. In addition it can be noticed that the implementation of an IG sequence has a beneficial impact

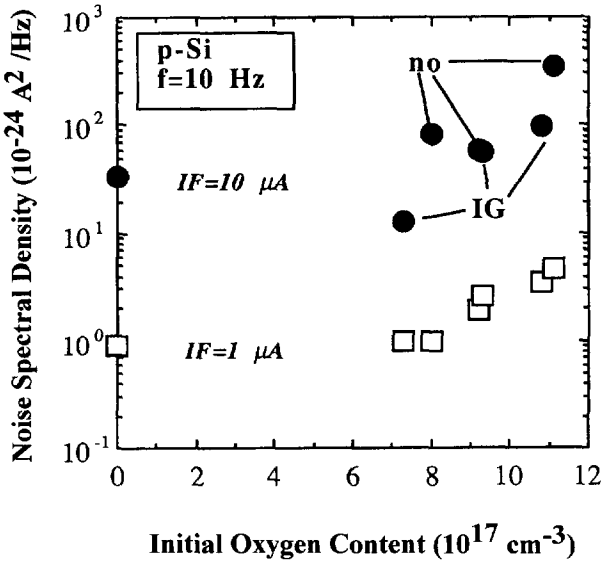

Fig. 9. — Correlation between the current noise spectral density measured at $f = 10$ Hz and the initial oxygen content of the substrates used for the fabrication of the n^+p diodes. The noise is measured at two different current levels.

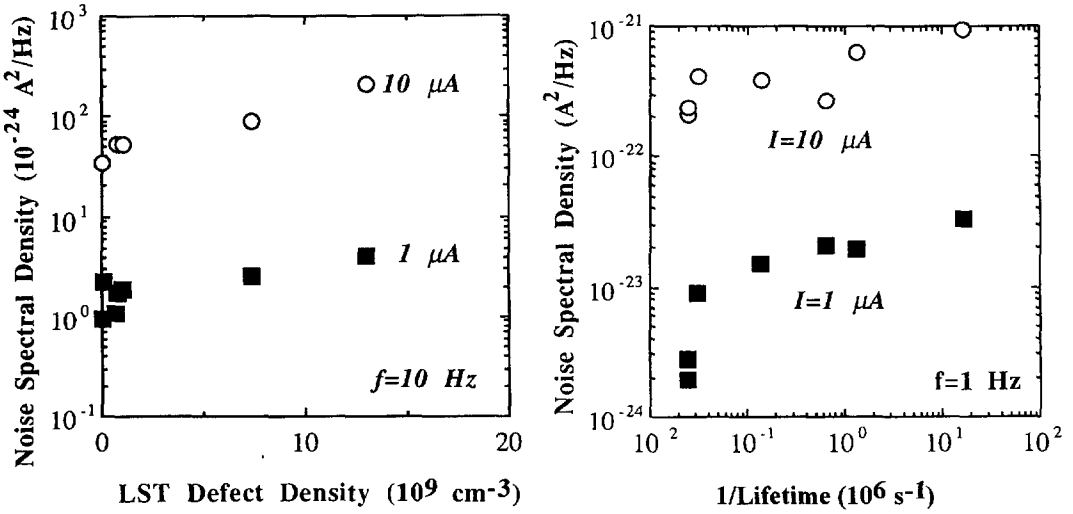

a) b)

Fig. 10 — a) Correlation between the current noise spectral density measured at $f = 10$ Hz and N_{LST} for n^+p diodes. $I_F = 1$ μA (■) and 10 μA (○) respectively. b) Correlation between the current noise spectral density measured at $f = 10$ Hz and the inverse recombination lifetime for n^+p diodes.

on the noise performance. It can generally be concluded that oxygen-precipitation induced defects have a strong impact on the LF noise behaviour.

3.3. DISCUSSION. — Structural analysis techniques such as FTIR, LST and TEM have been used to characterize the oxygen-precipitation related defects. Dependent on the used processing cycle, a near surface defect lean zone is formed. The observed infrared absorption peaks are in agreement with those reported in the literature for the SiO_x phase. Although still somewhat speculative, in some samples weak peaks may be associated with the formation of thermal donors. TEM and LST allow to determine the bulk defect density and in both cases the calculated densities are in close relation with each other. LST, however, has the main advantages that it is non-destructive, relatively fast and enables the detection of lower densities compared to TEM. On the other hand, TEM remains essential in case that an in depth structural identification of the defects is required.

The DLTS and diode evaluations point out that the electrical properties of oxide precipitates and their associated defect complexes are determined by the electron traps at $E_c - 0.23$ eV and $E_c - 0.43$ eV. Combining electrical with structural data, it is derived from Figure 4 that the deep levels found from DLTS or from the diode leakage current measurements show the same depth profile as for instance the oxygen-precipitation induced extended defects revealed by TEM. Furthermore, the data of Figure 7a strongly suggest that *not the total defect density* (*i.e.* from oxygen precipitates and associated extended defects) is of importance, *but the density of the dislocations and their state*, to explain the observed recombination activity. LST is mainly measuring the density of SiO_x precipitates. From this, it is concluded that the two electron traps found here are related to the electrical activity of the dislocations. The electrical activity is influenced by the core structure of the dislocations, their strain field, and their possible interactions with impurities. It can be noted that for instance Castaldini *et al.* [34], in their study of deformed FZ n-type Si, also observed two electron traps at very similar positions ($E_c - 0.18$ eV and $E_c - 0.4$ eV), which further supports the proposed identification. In general, clean dislocations are resulting in shallow levels, while in the presence of metallic contamination deep levels can be observed.

Based on standard SRH theory and the position of the trapping level in the bandgap, one can conclude that the bulk leakage current is determined by the $E_c - 0.43$ eV deep level. This is also in agreement with the above mentioned τ_g/τ_r ratio (Eq. (4)). Previous studies have also led to the conclusion that τ_g is dominated by a deep level around $E_c - 0.41$ [22] to $E_c - 0.47$ eV [35]. The recombination properties, on the other hand, appear to be determined by the shallow level. This follows both from the temperature dependent EBIC and MWA measurements, although one should also take the injection level dependence into consideration to get a clear picture in this matter [36].

The use of complementary analytical tool allows to obtain more information on different aspects of the oxygen-precipitation related extended defects. In this extensive study, which has been performed by using specially prepared and well characterized silicon wafers, none of the observed experimental data are in conflict with each other. Of key importance in this is to keep into account the sensitivity and the validity range of the different techniques. Based on the obtained insights, additional and well engineered processing experiments will be done in the future. A close interaction with silicon manufacturers has been established in order to be able to take also the crystal pulling parameters into account. Many of the apparently conflicting results reported in the literature are related to the fact that in the published experimental data, no information is given on the crystal pulling conditions and on the thermal history of the used silicon material. The concentration of grown-in point defects (vacancies and interstitials) strongly depends on the pulling conditions, while the thermal treatments of the pulled crystals

(*e.g.* the soaking treatment in order to stabilise the thermal donor formation) have a direct impact on the defect behaviour.

4. Conclusion

A variety of complementary tools have been used to characterize the electrical and structural properties of oxygen-precipitation related extended defects, generated in a controlled manner in well characterized silicon material. The DLTS observations allow to conclude that the electrical properties of oxide precipitates and their associated extended defects are dominated by two electron traps at $E_c - 0.23$ eV and at $E_c - 0.43$ eV. Combining the electrical and structural data, it is postulated that these levels are most likely connected to the associated dislocations and not to the oxide precipitates themselves. At the same time, it is demonstrated that these levels dominate the electrical performance of diodes fabricated in these substrates and therefore should be well-controlled in order to optimise the device performance and yield. Although the sensitivity of various analytical tools is continuously improving, to investigate the electrical activity of the defects an analysis of the device and circuit performance remains the most powerful technique as it is directly related to the yield, quality and reliability. For the full identification and characterization of the substrate defects involved the availability of complementary analytical tools is a prerequisite. However, due to the complexity of the interpretation of the experimental data and the fact that a large number of sometimes unknown parameters are involved, different School of Thought on the electrical activity of extended defects will remain to exist for the coming years. It is therefore essential to use well characterized material, to work closely together with a silicon manufacturer, and to control all the details of the wafer processing steps.

Acknowledgments

The authors are indebted to a large number of people for performing some of the analyses, stimulating discussions, and the use of some co-authored results: at IMEC M. Libezny and M.-A. Trauwaert; at ISP Frankfurt/Oder (Germany) G. Kissinger, M. Kittler, H. Richter and W. Seifert; at the University of Gent (Belgium) P. Clauws and A. Blondeel; at the University of Vilnius (Lithuania) E. Gaubas and A. Kaniava; G Bosman at the University of Gainesville (USA) and A. Czerwinski at the Institute of Electron Technology in Warsaw (Poland) are acknowledged for their contributions to the LF noise work. Part of the work has been financed by the European Space Agency (ESA) under contract 8615/90/NL/NB(SC) and by the Belgian National Science Foundation (NFWO).

References

[1] Fuller C.S., Ditzenberger J.A., Hannay N.B. and Buehler E., Resistivity Changes in Silicon Induced by Heat Treatment, *Phys. Rev.* **96** (1954) 833-838.

[2] Newman R.C., Light Impurities and Their Interactions in Silicon, *Mat. Sci. Eng. B* **36** (1996) 1-12.

[3] Bender H. and Vanhellemont J., Oxygen in Silicon, in Handbook on Semiconductors, T.S. Moss and S. Mahajan, Eds. (Elsevier, New York, 1994) pp. 1637-1753.

[4] Hu S.M. and Patrick W.J., Effect of Oxygen on Dislocation Movement in Silicon, *J. Appl. Phys.* **46** (1975) 1869-1874.

[5] Schwuttke G.H., *J. Electrochem. Soc.* **108** (1961) 163-167.

[6] Fiermans L. and Vennik J., Precipitation Behaviour of Copper in Silicon Single Crystals, *Phys. Stat. Sol.* **12** (1965) 277-289.

[7] Ewe H., Gilles D., Hahn S., Seibt M. and Schröter W., Basic Mechanisms of Internal Gettering: Heterogeneous Precipitation of Cobalt and Nickel in Cz-Silicon, Semiconductor Silicon 1994, H.R. Huff, W. Bergholz and K. Sumino, Eds., PV 94-10 (Electrochem. Soc. Ser., Pennington, 1994) pp. 796-819.

[8] Baghdadi A., Bullis W.M., Croarkin M.C., Li Y-Z., Scace R.I., Series R.W., Stallhofer P. and Watanabe M., Interlaboratory Determination of the Callibration Factor for the Measurement of the Interstitial Oxygen Content of Silicon by Infrared Absorption, *J. Electochem. Soc.* **136** (1989) 2015-2024.

[9] Kissinger G., Vanhellemont J., Claeys C. and Richter H., Observation of Stacking Faults and Prismatic Punching Systems in Silicon by Light Scattering Tomography, *J. Cryst. Growth* **158** (1996) 191-196.

[10] Lightowlers E.C., Growth and Characterisation of Semiconductors, R.A. Stradling and P.C. Klipstein, Eds. (Adam Hilger, Bristol, 1990).

[11] Vaitkus J., Gaubas E., Jarasiunas K. and Petrauskas M., Mapping of GaAs and Si Wafer and Ion-Implanted Layer by Light-Induced Scattering and Absorption of IR-Light, *Semicond. Sci. Technol. A* **7** (1992) 131-136.

[12] Simoen E., Vanhellemont J., Kaniava A. and Claeys C., The Impact of Processing-Induced Defects on the Electrical Characteristics and the Degradation of Si n^+p Junctions, The Degradation of Electronic Devices Due to Device Operation as well as Crystalline and Process-Induced Defects, H.J. Queisser, J.E. Chung, K.E. Bean and T.J. Shaffner, Eds., PV 94-1 (Electrochem. Soc. Ser., Pennington, 1994) pp. 72-81.

[13] Vanhellemont J., Simoen E. and Claeys C., On the Extraction of the Minority Carrier Recombination Lifetime from Forward Diode Characteristics, *Appl. Phys. Lett.* **66** (1995) 2894-2896.

[14] Kittler M, Lärz J., Morgenstern G. and Seifert W., Characterization of Polycrystalline Silicon by EBIC, *J. Phys. IV* **1** (1991) 173-179.

[15] Simoen E., Bosman G., Vanhellemont J. and Claeys C., Impact of the Substrate on the Low-Frequency Noise of Silicon n^+p Junction Diodes, *Appl. Phys. Lett.* **66** (1995) 2507-2509.

[16] Tempelhoff K., Spiegelberg F., Gleichman R. and Wruck D., Precipitation of Oxgen in Dislocation Free Silicon, *Phys. Stat. Sol. (a)* **56** (1979) 213-223.

[17] Vanhellemont J., Simoen E., Bosman G., Claeys C., Kaniava A., Gaubas E., Blondeel A. and Clauws P., On the Electrical Activity of Oxygen-Related Extended Defects in Silicon, Semiconductor Silicon 1994, H.R. Huff, W. Bergholz and K. Sumino, Eds., PV 94-10 (Electrochem. Soc. Ser., Pennington, 1994) pp. 670-683.

[18] Vanhellemont J., Libezny M., Simoen E., Claeys C., Clauws P. and Blondeel A., Spectroscopic Study of Oxygen Related Lattice Defects in Annealed Silicon, Proc. 22nd Int. Conf. on The Physics of Semiconductors, D.J. Lockwood, Ed. (World Scientific, Singapore, 1994) pp. 2399-2402.

[19] Vanhellemont J., Simoen E., Kaniava A., Libezny M. and Claeys C., Impact of Oxygen Related Extended Defects on Silicon Diode Characteristics, *J. Appl. Phys.* **77** (1995) 5669-5676.

[20] Kissinger G., Vanhellemont J., Gräf D., Zulehner W., Claeys C. and Richter H., Investigation of Crystal Defects in As-Grown and Processed Silicon Wafers and Heteroepitaxial layers by infrared Light Scattering Tomography, Analytical Techniques for Semiconductor Materials and Process Characterisation II (ALTECH 95), B.O. Kolbesen, C. Claeys and P. Stallhofer, Eds., PV 95-30(Electrochem. Soc. Ser., Pennington, 1995) pp. 156-165.

[21] Vanhellemont J., Kaniava A., Libezny M , Simoen E., Kissinger G., Gaubas E., Claeys C. and Clauws P., On the Recombination Activity of Oxygen Precipıtation Related Lattice Defects in Silicon, *Mat. Res. Soc. Symp.* **378** (1995) 35-40.

[22] Chan S.S., Varker C.J., Whitfield J.D. and Carpenter R.W., Deep Levels Associated with Oxygen Precipitation in CZ Silicon and Correlation with Minority Carrier Lifetime, *Mat. Res. Soc. Symp. Proc.* **46** (1985) 281-286.

[23] Libezny M., Kaniava A., Kissinger G., Nıjs J., Claeys C. and Vanhellemont J., PL Study of Oxygen Related Defects in Silicon, Analytical Techniques for Semiconductor Materials and Process Characterisation II (ALTECH 95), B.O. Kolbesen, C. Claeys and P. Stallhofer, Eds., PV 95-30(Electrochem. Soc. Ser., Pennington, 1995) pp. 166-173

[24] Weronek K., Weber J. and Queısser H.J., Hydrogen Passivation of the Dislocation-Related D-Band Luminescence in Silicon, *Phys Stat. Sol. (a)* **137** (1993) 543-548.

[25] Lelikov Y., Rebane Y., Ruvimov S., Tarhin D., Sitnikova A. and Schreter Y., Photoluminescence and Electronic Structure of Dislocations in Si Crystals, *Mat. Scı. For.* **83-87** (1992) 1321-1326.

[26] Wijaranakula W., A Quantitative Model for an Interaction Between Extended Dislocation Loops and Impurities in Czochralski Sılicon Based Upon the Photoluminescence Analysis, *J. Appl. Phys.* **70** (1991) 3018-3024.

[27] Schroder D.K., Semiconductor Materials and Device Characterization (Wiley, New York, 1990).

[28] Schroder D.K., Hwang J.M., Kang S.J., Goodman A.M. and Sopori B.L., Lifetime and Recombination Concepts for Oxygen-Precipitated Silicon, VLSI Science and Technology/1985, W.M. Bullis and S. Broydo, Eds., PV 85-5 (Electrochemical Soc. Ser., Pennington, 1995) pp. 419-428.

[29] Seifert W., Kittler M., Vanhellemont J , Simoen E., Claeys C. and Kirscht F.G., Recombination Activity of Oxygen Precipitation Related Defects in Silicon, Inst. Phys. Conf. Ser. (IOP Publ. Ltd) 149 149 (1996) 319-324.

[30] Kittler M., Ulhaq-Bouillet C. and Higgs V., Influence of Copper Contamination on Recombination Activity of Misfit Dislocations in SiGe/Si Epilayers: Temperature Dependence of Activity as a Marker Characterizing the Contamination Level, *J Appl. Phys.* **78** (1995) 4573-4583.

[31] Simoen E., Vanhellemont J., Rotondaro A.L.P. and Claeys C., Static and Low-Frequency Noise Characteristics of n^+p Junction Diodes Fabricated in Different Silicon Substrates, *Semıcond. Scı. Technol.* **10** (1995) 1002-1008.

[32] Simoen E., Vanhellemont J. and Claeys C., The Low-Frequency Noise Behaviour of Sı n^+p Junction Diodes Fabricated in (100) and (111) Substrates, *Inst. Phys. Conf. Ser.* N°149 (1996) 133-138.

[33] Simoen E., Vanhellemont J., Bosman G., Czerwinski A. and Claeys C., Extended Defect Related Excess Low-Frequency Noise in Si Junction Diodes, Inst. Phys. Conf. Ser. (IOP Publ. Ltd) 149 (1996) 133-138.

[34] Castaldını A., Cavalcoli D. and Cavallini A., Processing Effects on the Electrical Properties of Defects in Silicon, *Mat. Scı. and Eng. B* **4** (1989) 343-346.

[35] Kim H.S., Kim E.K. and Mın S.-K., Effects of Electron Deep Traps on Generation Lifetime in Denuded Zone of n-Type Si Wafer, *J. Appl. Phys.* **69** (1991) 6979-6981.

[36] Bullis W.M. and Huff H.R., Interpretation of Carrier Recombination Lifetime and Diffusion Length Measurements ın Silicon, *J. Electrochem. Soc.* **143** (1996) 1399-1405.